Observer Design for Reverse Flow Reactor

D. Edouard and D. Schweich
LGPC-CNRS, CPE-Lyon, Bat. 308 F, 43 Bd du 11 Novembre 1918, 69616 Villeurbanne Cedex, France

H. Hammouri
LAGEP, UMR 5007, UCBL I, CPE-Lyon, Bat. 308G, 43 Bd du 11 Novembre 1918, 69616 Villeurbanne Cedex, France

DOI 10.1002/aic.10128
Published online in Wiley InterScience (www.interscience.wiley.com).

A medium-scale reverse flow reactor for VOC combustion is considered. Heat loss and forced dilution by fresh air at the core of the reactor are accounted for. A countercurrent pseudohomogeneous model with frequency correction is proposed. This model is then used to synthesize an observer. This observer allows an on-line inlet estimate of inlet VOC concentration, and of the temperature profiles in the monoliths. © 2004 American Institute of Chemical Engineers *AIChE J,* 50: 2155–2166, 2004
Keywords: reverse flow reactor; VOC combustion; transient state; countercurrent model; pseudohomogeneous model; observer

Introduction

The catalytic reverse flow reactor (RFR) technology is especially efficient for purification of air containing volatile organic compounds (VOC) at low concentration: owing to the periodic flow reversals, a hot zone develops in the middle of the reactor where the combustion takes place. In addition to the intrinsically transient behavior of the RFR, one must deal with unexpected external disturbances (inlet VOC concentration, temperature, and so on), which may lead to extinction or catalyst overheating (aging or destruction). It is, thus, necessary to implement some closed-loop control strategy to avoid these problems. Inlet concentration disturbances can be easily detected using a total carbon analyzer, which is an expensive sensor. Since the RFR behaves as an "amplifier" of the adiabatic temperature rise, one may use some judiciously located thermocouples to observe the feed composition. A model-based soft sensor that quickly estimates the feed composition from three measured temperatures is discussed.

Experimental and theoretical investigations of the RFR have been presented in many publications. Most of them deal with the (periodic) steady state and its properties, such as stability or the extinction limit (van de Beld and Westerterp, 1994a, 1996; van de Beld et al., 1994b; Eigenberger and Nieken, 1988; Nieken et al., 1994a; Kolios et al., 2000; Züfle and Turek, 1997). In 1995, Nieken et al. proposed the countercurrent reactor analogy that describes the periodic steady state. This analogy allows describing the RFR under constant external conditions by a true steady-state model. Few articles are devoted to the transient state induced by external disturbances. Some deal with practical and technical issues (Cittadini et al., 2001, 2002), other with more theoretical problems (Garg et al., 2000). Most of these articles deal with the "ideal case," that is, adiabatic conditions and no dilution by fresh air at the center of the RFR. Matros and coworkers (see Matros and Buminovich, 1996) dealt with some nonideal situations. Kinhast et al. (1999) and Garg et al. (2000) dealt with heat loss, and showed that the RFR may exhibit nonsymmetric or chaotic temperature profiles. Heat removal or addition was investigated by Nieken et al. (1994) and Cunill et al. (1997) for control purposes. Finally, Ramdani et al. (2001) characterized the long-term dynamics due to external disturbances in the presence of heat loss and dilution by fresh air.

Deriving a soft sensor from a detailed model accounting for heat loss through the reactor wall, finite reversal frequency, reaction kinetics, and so on, is an overwhelming task and would be much time consuming on the computer. Thus, we propose to use the extended version of Ramdani et al. (2001) of the countercurrent reactor model with the following assumptions:

Correspondence concerning this article should be addressed to D. Edouard at edd@lobivia.cpe.fr.

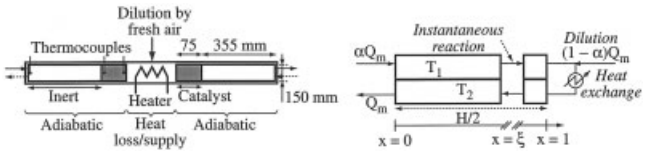

Figure 1. Left: Geometrical characteristics of the RFR; right: countercurrent model.

• The reaction is instantaneous and under mass-transfer control. This assumption implies that it will be impossible to predict the extinction phenomenon. Conversely, the model is independent of any chemical kinetic data.

• Heat loss takes place only in the central chamber of the RFR between the upstream and downstream monoliths (see Figure 1). This chamber behaves as a CSTR.

• Fresh air is injected in the central chamber where an electrical heater is located. Both can be used for temperature control purpose.

Using the countercurrent reactor analogy without heat loss means that the temperature profiles are "symmetrical" except where the reaction takes place. However, it is known that heat loss all along the RFR can be responsible for nonsymmetrical or chaotic profiles, especially at high reversal frequency. Since heat loss takes place at the center of the RFR only, we assumed that these nonusual profiles are not observed, although this would deserve a dedicated study. We will first derive the simplest model, which is pseudohomogeneous and involves only the solid temperature. We will then propose a simple correction for the finite flow reversal frequency. Finally, we will describe the observer which allows estimating the temperature profile and the unknown pollutant concentration. This observer is based on three measurements: the temperature at the inlet of the RFR, the temperatures at the inlet, and the outlet of the upstream catalytic monolith.

Pseudohomogeneous Model

Figure 1 shows the system under study and of the corresponding model. The "packing" is made of two sets of monoliths (1 mm square channels): a long inert monolith and a short catalytic one. The wide square crosssection of the monoliths prevents heat loss over their whole length (see Ramdani et al., 2001). Conversely, heat loss through the reactor wall takes place between the monoliths in the central chamber where the electrical heater is located, and where fresh air is injected. The basic balance equations for the countercurrent model are

$$\begin{cases} \lambda_{ax}^{s}\dfrac{\partial^2 T_s}{\partial z^2}+\dfrac{ha_c}{2}(T_1+T_2-2T_s)+a_c(-\Delta H)\dfrac{r_{s1}+r_{s2}}{2}=(1-\varepsilon)\rho_s c_{ps}\dfrac{\partial T_s}{\partial t} \\ \alpha\rho_0 u_{v0} c_{pmg}\dfrac{\partial T_1}{\partial z}+ha_c(T_1-T_s)=0,\ \alpha\rho_0 u_{v0}\dfrac{\partial \omega_1}{\partial z}+k_D a_c\rho(\omega_1-\omega_{1su})=0 \\ -\rho_0 u_{v0} c_{pmg}\dfrac{\partial T_2}{\partial z}+ha_c(T_2-T_s)=0,\ -\rho_0 u_{v0}\dfrac{\partial \omega_2}{\partial z}+k_D a_c\rho(\omega_2-\omega_{2su})=0 \\ k_D(\omega_1-\omega_{1su})=M\dfrac{r_{s1}}{\rho},\ k_D(\omega_2-\omega_{2su})=M\dfrac{r_{s2}}{\rho} \end{cases} \tag{1}$$

Under strong mass-transfer limitation, ω_{1su} and ω_{2su} can be neglected with respect to ω_1 and ω_2, respectively. Normalizing some variables and assuming that the Nusselt and Sherwood numbers on one hand, and the Schmidt and Prandtl numbers on the other hand, are equal, gives $h = k_D\rho c_{pmg}$ and

$$\begin{cases} (a)\quad \dfrac{1}{P_{ax}}\dfrac{\partial^2 T_s}{\partial x^2}+P\dfrac{(T_1+T_2-2T_s)}{2}+P\Delta T_{ad}\dfrac{\omega_1+\omega_2}{2\omega_{10}}\varphi(x)=\tau\dfrac{\partial T_s}{\partial t} \\ (b)\quad \alpha\dfrac{\partial T_1}{\partial x}+P(T_1-T_s)=0,\ -\dfrac{\partial T_2}{\partial x}+P(T_2-T_s)=0 \\ (c)\quad \alpha\dfrac{\partial \omega_1}{\partial x}+P\omega_1=0,\ -\dfrac{\partial \omega_2}{\partial x}+P\omega_2=0 \\ (d)\quad P=\dfrac{ha_c H}{2\rho_0 u_{v0} c_{pmg}},\ \dfrac{1}{P_{ax}}=\dfrac{2\lambda_{ax}^{s}}{H\rho_0 u_{v0} c_{pmg}},\ \tau=\dfrac{(1-\varepsilon)\rho_s c_{ps} H}{2\rho_0 u_{v0} c_{pmg}} \\ (e)\quad \Delta T_{ad}=\dfrac{\Delta H}{Mc_{pmg}}\omega_{10} \end{cases} \tag{2}$$

where $\varphi(x)$ accounts for the type of monoliths: $\varphi(x) = 0$ in the inert monoliths ($x < \xi$) and $\varphi(x) = 1$ in the catalytic monoliths ($x \geq \xi$). The boundary conditions are

$$\begin{cases} x = 0,\ \omega_1 = \omega_{10},\ T_1 = T_0,\ \dfrac{\partial T_s}{\partial x} = 0 \\ x = 1,\ \alpha\omega_1 = \omega_2,\ (1 + N')(T_2 - T_0) = \alpha(T_1 - T_0) + \dfrac{q_{ext}}{\rho_0 u_{v0} c_{pmg} S},\ \dfrac{\partial T_s}{\partial x} = 0 \end{cases} \tag{3}$$

where N' is the number of transfer units that accounts for heat loss in the central chamber. Assuming P to be uniform over x, Eqs. 2c yield

$$\begin{cases} \omega_1 = \omega_{10} e^{-P(x-\xi)/\alpha} \text{ for } x > \xi, \text{ and } \omega_1 = \omega_{10} \text{ for } x \le \xi \\ \omega_2 = \alpha\omega_{10} e^{-P((1-\xi)/\alpha + 1 - x)} \text{ for } x > \xi \text{ and } \omega_2 = \alpha\omega_{10} e^{-P((1-\xi)/\alpha + 1 - \xi)} \text{ for } x \le \xi \end{cases} \tag{4}$$

This shows that $\psi(x) = \varphi(x)[(\omega_1 + \omega_2)/2\omega_{10}]$ is a known function of α, P, x and ξ only. Typical values of P, α and ξ are 74, 0.95 and 0.826 respectively.

The pseudohomogeneous model is obtained using the method described by Balakotaiah and Dommeti (1999). Equations 2b are inverted using a formal development

$$\begin{cases} T_1 = \left(\dfrac{\alpha}{P}\dfrac{\partial}{\partial x} + I\right)^{-1} T_s = T_s + \displaystyle\sum_{k=1}^{\infty} \left(-\frac{\alpha}{P}\right)^k \frac{\partial^k T_s}{\partial x^k} \\ T_2 = \left(\dfrac{-1}{P}\dfrac{\partial}{\partial x} + I\right)^{-1} T_s = T_s + \displaystyle\sum_{k=1}^{\infty} \left(\frac{1}{P}\right)^k \frac{\partial^k T_s}{\partial x^k} \end{cases} \tag{5}$$

Equations 5 can also be obtained by successive derivations and substitution back into Eq. 2b. Since P is much greater than unity (typically, $P > 40$), we can truncate the development at the second-order term which leads to the following approximation

$$\begin{cases} T_1 \simeq T_s - \dfrac{\alpha}{P}\dfrac{\partial T_s}{\partial x} + \left(\dfrac{\alpha}{P}\right)^2 \dfrac{\partial^2 T_s}{\partial x^2} \\ T_2 \simeq T_s + \dfrac{1}{P}\dfrac{\partial T_s}{\partial x} + \left(\dfrac{1}{P}\right)^2 \dfrac{\partial^2 T_s}{\partial x^2} \end{cases} \tag{6}$$

This truncation conflicts with that used for obtaining Eq. 7. However, numerical simulations showed that it was sufficient.

The pseudohomogeneous model is finally given by Eqs. 7 and 9. Following the method of Balakotaiah and Dommeti (1999), it can be shown that the asymptotic developments (Eq. 5) converge provided that $P > 1$, which is the usual case.

Combining Eqs. 6 and 2a, we obtain the following homogeneous model described by a single heat balance equation

$$\left(\frac{1}{P_{ax}} + \frac{1 + \alpha^2}{2P}\right)\frac{\partial^2 T_s}{\partial x^2} + \frac{1 - \alpha}{2}\frac{\partial T_s}{\partial x} + P\Delta T_{ad}\psi(x) = \tau\frac{\partial T_s}{\partial t} \tag{7}$$

The first term of Eq. 7 involves an effective axial heat conductivity that is given by

$$\begin{cases} \dfrac{1}{P_{ax}} + \dfrac{1 + \alpha^2}{2P} = \dfrac{\lambda_{eff}}{\rho_0 u_{v0} c_{pmg} H/2} \\ \lambda_{eff} = \lambda_{ax}^s + \dfrac{1 + \alpha^2}{2}\dfrac{(\rho_0 u_{v0} c_{pmg})^2}{h a_c} \end{cases} \tag{8}$$

When $\alpha = 1$ (no dilution, see Figure 1), λ_{eff} reduces to the well-known estimate of Vortmeyer and Schäfer (1974) as used by Nieken et al. (1995).

Homogenizing the boundary conditions given by Eq. 3 is not that simple. Let us first remark that there are more conditions than required by Eq. 7. The condition over $\psi(x)$ (that is, ω_1 and ω_2) is approximated as told above: $\psi(x) = 0$ at $x = 0$ and $x = 1$. The condition over $T_s[(\partial T_s/\partial x) = 0]$ is ignored. Finally, the conditions over T_1, T_2 and T_s are expressed using Eq. 5 and truncating the developments above $1/P$

$$\begin{cases} T_s - \dfrac{\alpha}{P}\dfrac{\partial T_s}{\partial x} = T_0, \qquad \text{at } x = 0 \\ (1 + N')\left(T_s + \dfrac{1}{P}\dfrac{\partial T_s}{\partial x} - T_0\right) = \alpha\left(T_s - \dfrac{\alpha}{P}\dfrac{\partial T_s}{\partial x} - T_0\right) + \dfrac{q_{ext}}{\rho_0 u_{v0} c_{pmg} S} \quad \text{at } x = 1 \end{cases} \tag{9}$$

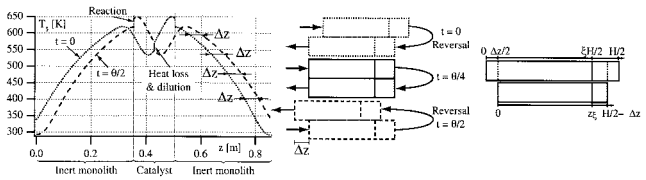

Figure 2. Left: Almost symmetric temperature profiles just before flow reversal. Middle: sliding countercurrent monoliths that superimpose the solid temperature profiles; right: truncated nonsliding "equivalent" monoliths.

Approximate Finite Frequency Model

The finite frequency in the RFR is responsible for a deviation with respect to the prediction based on the countercurrent model. To our knowledge, there is no simple method to account for the finite frequency except using a detailed and time-consuming model. We thus propose a simple approximation based on physical arguments. During a period θ, the solid temperature profile moves back and forth; it is almost symmetrical except where the reaction takes place close to $x = \xi$. At that location, the temperature profile can be relatively flat in the downstream monolith, or it can exhibit a temperature overshoot of ΔT_{ad} at most in the upstream monolith, where the (instantaneous) reaction takes place. Knowing that the temperature rise from $x = 0$ to $x = 1$ (adiabatic system, no dilution, that is, $N' = 0$ and $\alpha = 1$) is of the order $P\Delta T_{ad} \gg \Delta T_{ad}$, it is reasonable to assume that the solid temperature follows an oscillating and rather symmetrical profile within less than $\Delta T_{ad}/2$. The smaller the period, the more accurate the approximation would be. Figure 2 (left) illustrates this symmetry; the profiles were obtained with a detailed model as those described in the literature (see van de Beld and Westerterp, 1996; Nieken et al., 1995; Cittadini et al., 2001, 2002).

In the countercurrent model, the solid temperature profile is identical in the upstream and downstream monoliths by definition. To obtain this identity in the RFR at finite frequency, one must shift one monolith with respect to the other (Figure 2, middle). On a first approximation, one may thus consider that the RFR at finite frequency behaves as a "sliding countercurrent reactor." At flow reversal, the monoliths are shifted over a distance $\Delta z = v_T\theta/2$, where v_T is the propagation velocity of the temperature wave. Ignoring dilution and assuming that $T_{\max} - T_0$ is much greater than ΔT_{ad}, we have

$$v_T = \frac{H/2}{\tau}, \quad \Delta z = v_T\frac{\theta}{2} = \frac{H/2}{\tau}\frac{\theta}{2}, \quad \Delta x = \frac{\Delta z}{H/2} = \frac{\theta}{2\tau} \tag{10}$$

On a time average basis over half a period, two parts of length $\Delta z/2$ on both sides of the upstream monolith are not in contact with the downstream monolith. If we assume that these parts do not contribute to the heat storage process, then the system behaves as a countercurrent reactor with nonsliding truncated monoliths of length equal to the average length of the parts in contact (see Figure 2). The real size $H/2$ is, thus, reduced by $\Delta z/2$ on both extremities. This means that the corrected P and ξ are given by P_θ and ξ_θ

$$\begin{cases} P_\theta = \dfrac{ha_c}{\rho_0 u_{s0} c_{pmg}}(H/2 - \Delta z) = P(1 - \Delta x) \\ \dfrac{1}{P_{ax\theta}} = \dfrac{\lambda_{ax}}{\rho_0 u_{s0} c_{pmg} H/2(1 - \Delta x)} \\ z_{\xi_\theta} = \xi\dfrac{H}{2} - \dfrac{\Delta z}{2} \\ \xi_\theta = \dfrac{z_\xi}{H/2 - \Delta z} = \dfrac{\xi - \Delta x/2}{1 - \Delta x} \end{cases} \tag{11}$$

These simple estimates hold, provided that $0 < \xi\theta < 1$, that is, $\theta/4\tau < \text{Max}(\xi, 1 - \xi)$. Figure 3 compares the results of an experiment at the periodic steady state, with those of a detailed model accounting for the finite frequency and of the pseudohomogeneous model when P_θ and ξ_θ are substituted for P and ξ. The agreement is excellent, and it will be assumed that the pseudohomogeneous model together with Eq. 11 is still valid in the long term transient state due to forced dilution, heat supply, and feed composition changes. We remark that the feed composition ω_{10} is involved only through ΔT_{ad} (see Eq. 2e). This means that ΔT_{ad} is the basic feed disturbances that needs to be estimated.

High Gain Observer

In practice, a model-based control or supervision strategy requires knowledge of the state of the process. One way permitting to obtain such unknown state consists in using physical sensors. However, in many cases, due to cost consideration and physical constraints, the number and types of sensors remain very limited. To cure this problem, one solution is to design an observer. This method combines *a priori* knowledge about a physical system (nominal model) with experimental data (some on-line measurements) to provide an on-line estimation of states and/or parameters. Among these algorithms, the Kalman filter is often proposed in the literature. However, this filter requires solving a dynamical Riccati equation, which is nonlinear. Beside some numerical difficulty, the dimension of the Riccati equation becomes very large: $(n^2 + n)/2$, if n is the dimension of the state vector that has to be estimated (in our

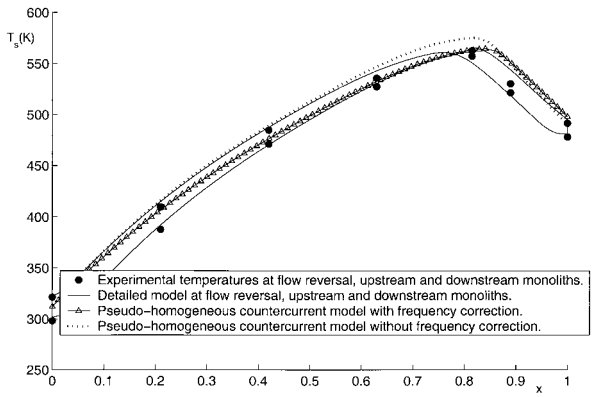

Figure 3. Comparison between an experiment, a detailed model and the pseudohomogeneous countercurrent model with frequency correction.

$\theta = 16$ s, $P = 73.9$, $\Delta T_{ad} = 25$ K, $\tau = 143$ s, $\xi = 0.826$, $\alpha = 0.95$, $N' = 0.035$.

case $n = 200$). The latter fact renders the on-line estimation very time consuming. Our approach consists in designing a simple observer. This observer derives from the high gain techniques (see for example, Bornard and Hammouri, 1991; Deza et al., 1992; Farza et al., 1998; Gauthier et al., 1992; Gauthier and Kupka, 1994). The gain of the proposed observer doesn't require solving any differential equation, and its calibration is very simple. This section is organized as follows: First, we use the finite difference method to approximate the model Eqs. 7, 9, and 11 by an ordinary differential system of finite dimension. Next, the resulting model is reordered in order to obtain a particular structure permitting to synthesize an observer, which allows estimating the temperature profile together with the pollutant concentration.

Space discretization: Finite difference method

The normalized space domain of the partial differential Eq. 7, 9 is [0, 1], the space variable is denoted by x, $x \in [0, 1]$. The discretization points are denoted by x_i. In order to obtain a satisfactory temperature profile, simulations require 200 points. The same number of points has been considered both in the inert and in catalytic monoliths (that is, 100, 100), leading to different space discretization. $\Delta x_k = x_i - x_{i-1}$ for $1 \leq i \leq 201$ and $x_0 = 0$, $x_{201} = 1$ (where $k = 1$ corresponds to the inert monolith, $k = 2$ corresponds to the catalytic monolith). $T_s(x_1, t), \ldots, T_s(x_{100}, t)$ correspond to the discretized temperature profile in the inert monolith, and $T_s(x_{101}, t), \ldots, T_s(x_{200}, t)$ are the temperatures of the reactive one. The finite difference method is based on the following formulas

$$
\begin{aligned}
i \neq 101 \rightarrow & \begin{cases} \left.\dfrac{\partial T_s(x,t)}{\partial x}\right|_i = \dfrac{T_s(x_i,t) - T_s(x_{i-1},t)}{\Delta x_k} \\ \left.\dfrac{\partial^2 T_s(x,t)}{\partial x^2}\right|_i = \dfrac{T_s(x_{i+1},t) - 2T_s(x_i,t) + T(x_{i-1,t})}{\Delta x_k^2} \end{cases} \\
i = 101,\ x_{101} = \xi_\theta \rightarrow & \begin{cases} \left.\dfrac{\partial T_s(x_{101},t)}{\partial x^2}\right|_{x_{101}} = \dfrac{T_s(x_{101},t) - T_s(x_{100},t)}{\Delta x_1} \\ \left.\dfrac{\partial^2 T_s(x_{101},t)}{\partial x^2}\right|_{x_{101}} = \dfrac{T_s(x_{102},t)}{\Delta x_2^2} - \dfrac{(\Delta x_1 + \Delta x_2) T_s(x_{101},t)}{\Delta x_2^2 \Delta x_1} + \dfrac{T_s(x_{100},t)}{\Delta x_1 \Delta x_2} \end{cases}
\end{aligned}
\tag{12}
$$

The temperatures at x_0 and x_{201} are given by the boundary conditions (see Eq. 9).

On-line estimation of the temperature profile and of the unknown pollutant concentration

The supervision and the control of the RFR process generally requires knowledge of the pollutant concentration, and of the temperature profile inside the reactor. Here, the pollutant concentration is considered as an unknown disturbance. From the proportionality relationship between the adiabatic temperature rise and the VOC concentration (see Eq. 2e), we only need to estimate ΔT_{ad}. We will assume that ΔT_{ad} can be considered as the response of a second order system

$$
\begin{cases} \dfrac{d}{dt} \Delta T_{ad}(t) = \zeta(t) \\ \dfrac{d}{dt} \zeta(t) = v(t) \end{cases} \tag{13}
$$

where $v(t)$ is an unknown, but bounded signal. Noticing that this assumption is not a strong one. Indeed, any physical signal can be approximated by a response of such second-order filter.

The experimental temperatures used to feed the observer are chosen according to the following remarks:

- As shown in Figure 2, the inlet temperature of the upstream catalytic monolith is strongly sensitive to the reaction, that is, the pollutant concentration. However, this local temperature also depends on heat loss and the feed temperature.
- The temperature undershoot at the outlet of the upstream catalytic monolith is sensitive to heat loss in the central chamber.
- The temperature at the inlet of the reactor is the feed temperature.

Thus, it seems logical that these three temperature are the most appropriate for the observer. In practice, these measured temperatures are filtered using a sliding average over one period (see Figure 5, $(y_1(t), y_2(t), y_3(t))$, because the pseudohomogeneous model doesn't take into account the fast dynamics, due to the flow reversal.

The observer is derived from the high gain observer techniques (see Gauthier et al., 1992; Deza et al., 1992; Hammouri et al., 2002). The formulation of this observer requires a particular structure called triangular form. In order to obtain this triangular form, we use the following standard notations:

The discretized temperature profile in the nonreactive compartment will be denoted by the state vector

$$
X^1(t) = \begin{pmatrix} T_s(x_1,t) \\ \vdots \\ T_s(x_{100},t) \end{pmatrix} = \begin{pmatrix} X_1^1(t) \\ \vdots \\ X_{100}^1(t) \end{pmatrix},
$$

$X^2(t)$ denotes a three-dimensional (3-D) state vector

$$
\begin{pmatrix} X_1^2(t) \\ X_2^2(t) \\ X_3^2(t) \end{pmatrix},
$$

where, $X_1^2(t) = T_s(x_{101}, t)$, $X_2^2(t) = \Delta T_{ad}(t)$ and $X_3^2(t) = \zeta(t)$, where $\zeta(t)$ is the variable which appears in Eq. 13, and finally,

$$X^3(t) = \begin{pmatrix} T_s(x_{200}, t) \\ \vdots \\ T_s(x_{102}, t) \end{pmatrix} = \begin{pmatrix} X_1^3(t) \\ \vdots \\ X_{99}^3(t) \end{pmatrix}$$

The components of $X^3(t)$ together with $X_1^2(t) = T_s(x_{101}, t)$ constitute the discretized temperature profile in the reactive compartment. Let $y_1(t) = X_1^1(t) = T_s(x_1, t)$, $y_2(t) = X_1^2(t) = T_s(x_{101}, t)$ and $y_3(t) = X_1^3(t) = T_s(x_{200}, t)$ be the temperature measurements. The global extended model on which the observer is based, takes the following form

$$\begin{cases} \dot{X}^1(t) = A^1(t)X^1(t) + G^1(X^1(t), y_2(t), T_0, t) \\ \dot{X}^2(t) = A^2(t)X^2(t) + G^2(X^2(t), X_{99}^3(t), X_{100}^1(t), t) + v(t)B \\ \dot{X}^3(t) = A^3(t)X^3(t) + G^3(X^3(t), X_2^2(t), T_o, q_{ext}, y_2(t), t) \\ y_1(t) = C_1X^1(t) = X_1^1(t) \\ y_2(t) = C_2X^2(t) = X_1^2(t) \\ y_3(t) = C_3X^3(t) = X_1^3(t) \end{cases} \tag{14}$$

with

$$A^1(t) = a_1(t)\begin{pmatrix} 0 & 1 & 0 & 0 \\ \vdots & \ddots & \ddots & 0 \\ 0 & \vdots & \ddots & 1 \\ 0 & \cdots & \cdots & 0 \end{pmatrix};$$

$$A^2(t) = \begin{pmatrix} 0 & r(t) & 0 \\ 0 & 0 & 1 \\ 0 & 0 & 0 \end{pmatrix}; A^3(t) = a_3(t)\begin{pmatrix} 0 & 1 & 0 & 0 \\ \vdots & \ddots & \ddots & 0 \\ 0 & \cdots & \ddots & 1 \\ 0 & \cdots & \cdots & 0 \end{pmatrix}.$$

and

$$B = \begin{pmatrix} 0 \\ 0 \\ 1 \end{pmatrix}; C_1 = (1 \quad 0, \ldots, 0); C_2 = (1 \quad 0 \quad 0)$$

and

$$C_3 = (1 \quad 0, \ldots, 0)$$

The expressions of the G_i^j's are given in the Appendix. The dynamic structure (Eq. 14) is called a triangular structure. With this notation, the observer design takes the following form

$$\begin{cases} \dot{\hat{X}}^1(t) = A^1(t)\hat{X}^1(t) + G^1(\hat{X}^1(t), y_2(t), T_0, t) + a_1(t)\Theta_1K^1(\hat{X}_1^1(t) - y_1(t)) \\ \dot{\hat{X}}^2(t) = A^2(t)\hat{X}^2(t) + G^2(\hat{X}^2(t), \hat{X}_{99}^3(t), \hat{X}_{100}^1(t), t) + \Lambda(t)\Theta_2K^2(\hat{X}_1^2(t) - y_2(t)) \\ \dot{\hat{X}}^3(t) = A^3(t)\hat{X}^3(t) + G^3(\hat{X}^3(t), \hat{X}_2^2(t), y_2(t), T_0, q_{ext}, t) + a_3(t)\Theta_3K^3(\hat{X}_1^3(t) - y_3(t)) \end{cases} \tag{15}$$

where

$$K^1 = \begin{pmatrix} K_1^1 \\ \vdots \\ K_{100}^1 \end{pmatrix}, \quad K^2 = \begin{pmatrix} K_1^2 \\ K_2^2 \\ K_3^2 \end{pmatrix}$$

and

$$K^3 = \begin{pmatrix} K_1^3 \\ \vdots \\ K_{99}^3 \end{pmatrix}$$

are such that the matrices

$$\bar{A}^1 = \begin{pmatrix} K_1^1 & 1 & 0 & 0 \\ \vdots & 0 & \ddots & \vdots \\ K_{99}^1 & 0 & \cdots & 1 \\ K_{100}^1 & 0 & \cdots & 0 \end{pmatrix}, \quad \bar{A}^2 = \begin{pmatrix} K_1^2 & 1 & 0 \\ K_2^2 & 0 & 1 \\ K_3^2 & 0 & 0 \end{pmatrix},$$

$$\bar{A}^3 = \begin{pmatrix} K_1^3 & 1 & 0 & 0 \\ \vdots & 0 & \ddots & \vdots \\ K_{98}^3 & 0 & \cdots & 1 \\ K_{99}^3 & 0 & \cdots & 0 \end{pmatrix}$$

are stable (it means that the real part of the eigenvalues of the $\bar{A}^i$'s are negative). Θ_i are given by:

$$\Theta_1 = \begin{pmatrix} \Omega & 0 & 0 \\ 0 & \ddots & 0 \\ 0 & 0 & \Omega^{100} \end{pmatrix}; \Theta_2 = \begin{pmatrix} \Omega & 0 & 0 \\ 0 & \Omega^2 & 0 \\ 0 & 0 & \Omega^3 \end{pmatrix};$$

$$\Theta_3 = \begin{pmatrix} \Omega & 0 & 0 \\ 0 & \ddots & 0 \\ 0 & 0 & \Omega^{99} \end{pmatrix}.$$

$\Omega > 0$ is the parameter of calibration of the observer. This parameter must be judiciously chosen (see Figure 7). Finally,

$$\Lambda(t) = \begin{pmatrix} 1 & 0 & 0 \\ 0 & 1/r(t) & 0 \\ 0 & 0 & 1/r(t) \end{pmatrix}$$

The proof of the convergence of observer (Eq. 15) is given in the Appendix.

Implementation of the observer

The observer has been validated under the following conditions:

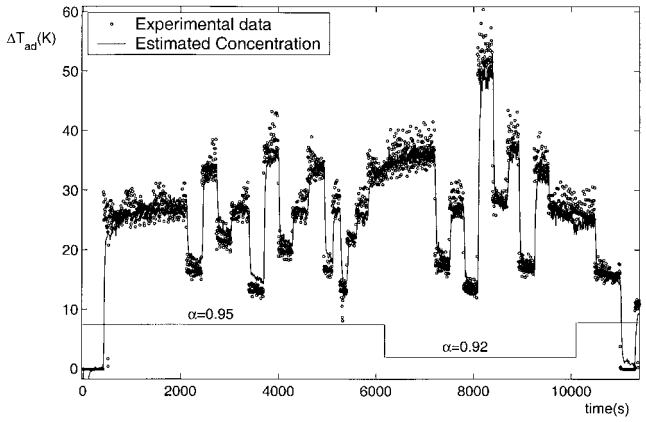

Figure 4. Comparison between the inlet experimental concentration and its corresponding on-line estimation.

- The reactor is ignited, and the external power supply is set to be $q_{ext} = 0$.
- The ratio of the feed flow rate $\alpha(t)$ is a time-varying signal, which takes its values in the interval [0.95, 0.92] (see Figure 4).
- The external temperature: $T_0 = 293$ K.
- The inlet concentration is considered as a disturbance (see Figure 4).
- Six thermocouples are inserted in certain channels. The sampling frequency is 0.25 Hz. Only three temperature measurements are necessary for the observer (see Figure 5). The three others are used to validate the observer's performance.
- No particular initial states are required for the implementation of the observer.
- The "Acker" subroutine existing in MATLAB (pole placement techniques), is used to obtain the K^i's.
- The choice of a satisfactory gain Ω is obtained from simulation. Indeed, many values of Ω have been tested in order to choose the best value of Ω, permitting to obtain a good performance of the observer. In our case, the best value corresponds to $\Omega = 3$ (see Figure 7).

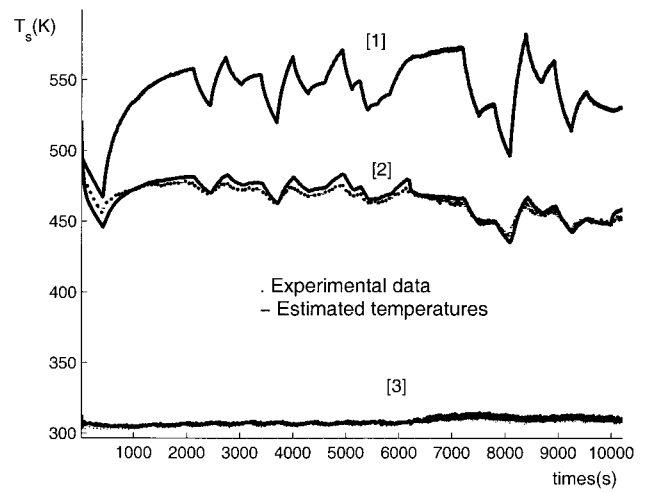

Figure 5. Filtered temperature measurements and their on-line estimation. $(y_2(t), \hat{T}_s(x_{101}, t)) = [1]$, $(y_3(t), \hat{T}_s(x_{200}, t)) = [2]$, $(y_1(t), \hat{T}_s(x_1, t)) = [3]$.

For curves [1] and [3] experimental and estimated data are superimposed.

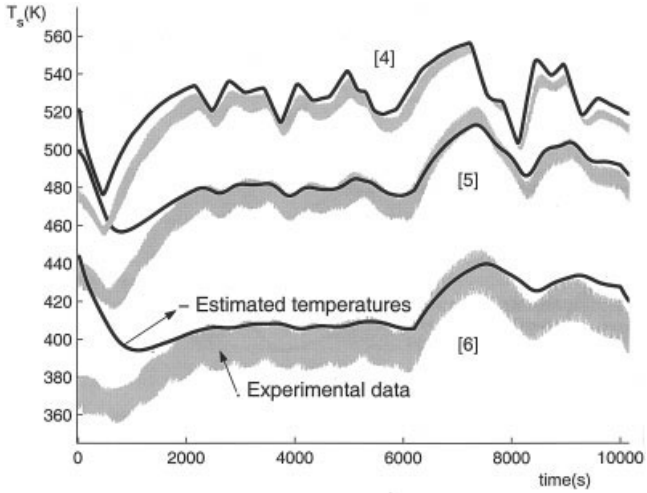

Figure 6. Experimental validation.

$(T_s(x_{25}, t), \hat{T}_s(x_{25}, t)) = [6]$, $(T_s(x_{50}, t), \hat{T}_s(x_{50}, t)) = [5]$, $(T_s(x_{75}, 7), \hat{T}_s(x_{75}, t)) = [4]$.

Experimental validation of the observer

The period of flow reversal is 16 s. The liquid pollutant (xylene) is pumped through a capillary tube into ambient air, where it vaporizes upstream of the RFR. Changing the liquid flow rate of xylene allows monitoring of the inlet VOC concentration. As mentioned earlier, this concentration is expressed as the adiabatic temperature rise (ΔT_{ad}) through Eq. 2e. Figure 4 compares the experimental ΔT_{ad} and its estimate. The stiff changes and the almost steady portions are well accounted for. The lid of the RFR is not perfectly airtight. As illustrated in Figure 1, a small amount of fresh air ($\alpha = 0.95$) is aspirated into the core. A valve connected to the core of the reactor allows adding further fresh air ($3m^3 \cdot h^{-1}$ STP or $\alpha = 0.92$) at $t = 6200$ s (Figure 4). The feed flow rate of liquid pollutant, and the outlet gas flow rate being constant, any fresh air addition is reflected in an increase of the inlet concentration, that is, ΔT_{ad}. This is readily observed on both the experimental and theoretical curves of Figure 4 at $t = 6200$ s. Note that for $\Delta T_{ad} \simeq 50$ K, the RFR must works under a forced dilution to prevent catalyst overheating. The measured and estimated temperatures are plotted versus time in Figure 5:

- at the boundary between catalytic and inert monoliths [1], the difference is less than 1 K.
- at the outlet catalytic monolith [2], the difference is less than 5 K.
- at the inlet inert monolith [3], the difference is less than 3 K.

These differences between the experimental measurements and their estimates are mainly due to the parametric uncertainty and the physical noise.

In order to check the convergence of our observer, we added three new thermocouples at different positions, namely, $T_s(x_{25}, t)$, $T_s(x_{50}, t)$ and $T_s(x_{75}, t)$ (see Figure 6). Note that these measurements are not filtered because they are not used

by the observer. However, they permit to show the quality of the intermediate temperature estimates. Although, the initial states $\hat{T}_s(x_{25}, 0)$, $\hat{T}_s(x_{50}, 0)$ and $\hat{T}_s(x_{75}, 0)$ are different from their corresponding experimental measurements, respectively, $T_s(x_{25}, 0)$, $T_s(x_{50}, 0)$, and $T_s(x_{75}, 0)$, the estimated variables $\hat{T}_s(x_{25}, t)$, $\hat{T}_s(x_{50}, t)$, and $\hat{T}_s(x_{75}, t)$ converge to the experimental temperature. The differences between experimental and estimated temperatures may be essentially attributed to the inaccurate location of the thermocouples.

In Figure 7, different values of the calibration parameter (Ω) are tested. According to the high gain observer theory (see Appendix), there is no convergence when $\Omega < 1$. In the case of to a high value of Ω ($\Omega = 11$), the observer performance is degraded due to the noise amplification. In our case study, the best value obtained from simulation corresponds approximately to $\Omega = 3$. For this value, the observer converges within 50 s. Note, that the response time of the system is approximately 1,000 s. The model ignores chemical kinetics limitation. Consequently, the observer can no longer estimates the feed concentration when extinction takes place. This is illustrated in Figure 8. In the corresponding experiment, the feed concentration is varied and then maintained ($t > 1.15 \times 10^4$ s) below the extinction limit (at steady state). As long as the reactor is ignited, ΔT_{ad} is well estimated. When extinction begins ($t \sim 1.35 \times 10^4$ s), the observer "believes" that the pollutant disappears.

Conclusions

The supervision and the control of the RFR require knowledge of the temperature profile, and of the pollutant concentration. Since, the maximum temperature is an image of this concentration, all the necessary information can be recovered from a few thermocouples suitably located, and using a soft sensor. This soft sensor is derived from a model that was simplified using a well-known analogy, and introducing two new tools:

- A robust homogenization method;
- A finite frequency correction.

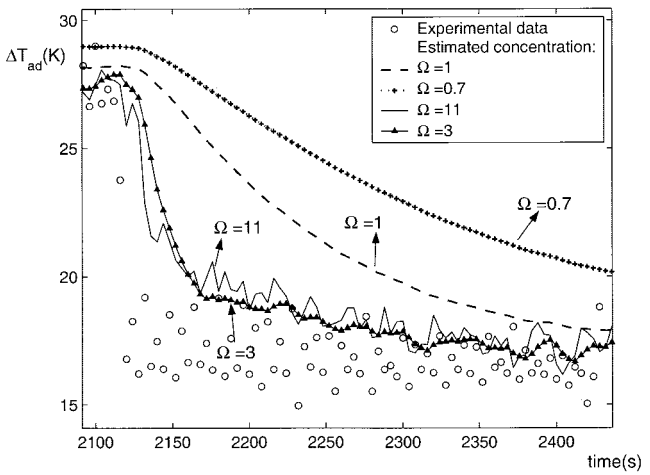

Figure 7. Inlet experimental concentration and inlet estimated concentration for different values of Ω.

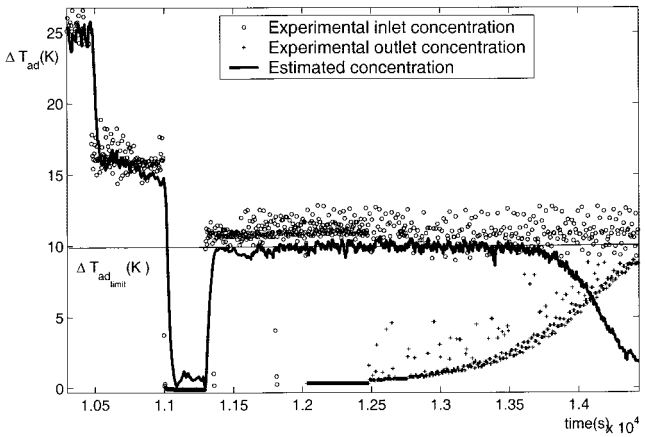

Figure 8. Limit of the observer: extinction of the reactor.

The resulting model can be put into the triangular structure required by the high gain observer theory. The result is a fast converging soft sensor, based on three temperature measures, that is of low computation cost. The sensor was successfully checked against experiments under various conditions provided that extinction does not take place. This observer will be used to control the RFR, and this will be the subject of a future article.

Notation

a_c = specific solid-fluid surface area, m^{-1}
c_{ps} = solid heat capacity, $J \cdot kg^{-1} \cdot K^{-1}$
c_{pmg} = fluid heat capacity, $J \cdot kg^{-1} \cdot K^{-1}$
H = total length of monolith, m
h = solid-fluid heat-transfer coefficient, $W \cdot m^{-2} \cdot K^{-1}$
k_D = solid-fluid mass transfer coefficient, $m \cdot s^{-1}$
M = VOC molecular weight, $kg \cdot mol^{-1}$
N' = number of transfer units for heat loss
P = Peclet number for solid-fluid heat transfer
P_{ax} = axial Peclet number for heat conduction
P_θ = P corrected for the finite frequency
q_{ext} = external power supply, W
r_{s1}, r_{s2} = rate of reaction in the upstream, downstream monolith, $mol \cdot m^{-2} \cdot s^{-1}$
S = total cross-section of the monolith, m^2
T_1, T_2 = gas temperature in the upstream, downstream monolith, K
T_0 = inlet and external temperature, K
T_{max} = maximum solid temperature in the RFR, K
T_s or T = solid temperature, K
t = time, s
u_{s0} = superficial gas velocity in the reference state, $m \cdot s^{-1}$
v_T = propagation velocity of the temperature wave, $m \cdot s^{-1}$
x = reduced abscissa, 2z/H
z = abscissa, m
α = fraction of feed flow rate
ΔH = reaction enthalpy, $J \cdot mol^{-1}$
ΔT_{ad} = adiabatic temperature rise, K
Δz = maximum shift of the temperature profile, m
Δx = reduced Δz
ε = fraction of open frontal area
$\varphi(x)$ = characteristic function of the catalytic monolith
$\psi(x)$ = $\varphi(x)(\omega_1 + \omega_2)/(2\omega_{10})$
λ^s_{ax} = solid axial conductivity, $W \cdot m^{-1} \cdot K^{-1}$
λ_{eff} = effective axial heat conductivity
ρ = fluid density, $kg \cdot m^{-3}$
ρ_0 = gas density in the reference state, $kg \cdot m^{-3}$
ρ_s = solid density, $kg \cdot m^{-3}$
τ = heat storage time constant, s
θ = period of flow reversal, s

ω_{1su}, ω_{2su} = VOC mass fraction of solid phase in the upstream, downstream monoliths
ω_1, ω_2 = VOC mass fraction in the upstream, downstream monoliths
ω_{10} = VOC mass fraction in the feed
ξ = reduced abscissa of the boundary between the inert and catalytic monoliths
ξ_θ = ξ corrected for the finite frequency
X = state vector
$\hat{X}$ = estimated state vector
y = filtered temperature measurements, K
Ω = calibration parameter of the observer

Literature Cited

Balakotaiah, V., and S. M. S. Dommeti, "Effective Models for Packed-Bed Catalytic Reactors," *Chem. Eng. Sci.,* **54**, 1621 (1999).

Bornard, G., and H. Hammouri, "A High Gain Observer for a Class of Uniformly Observable Systems," *Proc. of the 30th IEEE Conf. on Decision and Control,* Brighton, UK, p. 1494 (1991).

Cittadini, M., M. Vanni, and A. A. Barresi, "Transient Behavior and Start-Up of Periodic Flow Reversal Reactors for Catalytic Decontamination of Waste Gases," *Chem. Eng. Process.,* **41**, 437 (2002).

Cittadini, M., M. Vanni, A. A. Barresi, and G. Baldi, "Reverse-Flow Catalytic Burners: Response to Periodical Variations in the Feed," *Chem. Eng. Sci.,* **56**, 1443 (2001).

Cunill, F., L. van de Beld, and R. K. Westertep, "Catalytic Combustion of Very Lean Mixtures in Reverse Flow Reactor Using an Internal Heater," *Ind. Eng. Chem. Res.,* **36**, 4198 (1997).

Deza, F., E. Busvelle, and J. P. Gauthier, "High Gain Estimation for Nonlinear Systems," *Syst. & Cont. Letters,* **18**, 295 (1992).

Eigenberger, G., and U. Nieken, "Catalytic Combustion with Periodic Flow Reversal," *Chem. Eng. Sci.,* **43**(8), 2109 (1988).

Farza, M., H. Hammouri, and K. Busavon, "A Simple Observer for a Class of Nonlinear Systems," *Appl. Mat. Letters,* **11**, 27 (1998).

Garg, R., D. Luss, and J. G. Kinhast, "Dynamic and Steady State Features of a Cooled Countercurrent Flow Reactor," *AIChE J.,* **46**(10), 2030 (2000).

Gauthier, J. P., H. Hammouri, and S. Othman, "A Simple Observer for Nonlinear Systems, Application to Bioreactors," *IEEE Trans. Automat. Cont.,* **37**, 875 (1992).

Gauthier, J. P., and I. A. K. Kupka, "Observability and Observers for Nonlinear Systems," *SIAM J. Cont. and Optim.,* **32**, 975 (1994).

Hammouri, H., B. Targui, and F. Armanet, "High Gain Observer Based on a Triangular Structure," *Int. J. of Robust and Nonlinear Cont.,* **12**(6), 497 (2002).

Kinhast, J., Y. O. Jeong, and D. Luss, "Dependence of Cooled Reverse-Flow Reactor Dynamics on Reactor Model," *AIChE J.,* **45**(2), 299 (1999).

Kolios, G., J. Frauhammer, and G. Eigenberger, "Autothermal Fixed-Bed Reactors Concepts," *Chem. Eng. Sci.,* **55**, 5945 (2000).

Matros, Y. S., and G. A. Bunimovich, "Reverse Flow Operation in Fixed-Bed Catalytic Reactors," *Catal. Rev. Sci. and Eng.,* **38**(1), 1 (1996).

Nieken, U., G. Kolios, and G. Eigenberger, "Limiting Cases and Approximate Solutions for Fixed-Bed Reactors with Periodic Flow Reversal," *AIChE J.,* **41**(8), 1915 (1995).

Nieken, U., G. Kolios, and G. Eigenberger, "Fixed-Bed Reactors with Periodic Flow Reversal: Experimental Results for Catalytic Combustion," *Catalysis Today,* **20**, 335 (1994a).

Nieken, U., G. Kolios, and G. Eigenberger, "Control of the Ignited Steady State in Autothermal Fixed Bed Reactors for Catalytic Combustion," *Chem. Eng. Sci.,* **49**(24B), 5507 (1994b).

Ramdani, K., R. Pontier, and D. Schweich, "Reverse Flow Reactor at Short Switching Period for VOC Combustion," *Chem. Eng. Sci.,* **56**, 1531 (2001).

van de Beld, B., and K. R. Westerterp, "Air Purification by Catalytic Oxidation in a Reactor with Periodic Flow Reversal," *Chem. Eng. Technol.,* **17**, 217 (1994a).

van de Beld, B., R. A. Borman, O. R. Derkx, B. A. A. Van Woezik, and R. K. Westerterp, "Removal of Volatile Organic Compounds from Polluted Air in a Reverse Flow Reactor: An Experimental Study," *Ind. Eng. Chem. Res.,* **33**, 2446 (1994b).

van de Beld, B., and K. R. Westerterp, "Air Purification in a Reverse Flow Reactor: Model Simulations Versus Experiments," *AIChE J.,* **42**(4), 1139 (1996).

Vortmeyer, D., and R. J. Schfer, "Equivalence of One- and Two-Dimensional Models for Heat Transfer Processes in Packed Beds: One Dimensional Theory," *Chem. Eng. Sci.,* **29**, 485 (1974).

Züfle, H., and T. Turek, "Catalytic Combustion in a Reactor With Periodic Flow Reversal. Part 1. Experimental Results," *Chem. Eng. Process,* **36**, 327 (1997).

Appendix

The triangular form

From the model (Eqs. 7 and 9), and by using the finite difference method (Eq. 12), and the assumption on the modeling of the ΔT_{ad} (Eq. 13), our candidate observer will be based on the following discretized equations

$$\begin{cases} \dot{t}_s(x_1, t) = a_4(t)T_s(x_1, t) + a_1(t)T_s(x_2, t) + b_1(t)T_0 \\ \dot{T}_s(x_i, t) = a_3(t)T_s(x_{i-1}, t) + a_2(t)T_s(x_i, t) + a_1(t)T_s(x_{i+1}, t) \text{ for } 2 \le i \le 100 \end{cases} \tag{A1}$$

$$\begin{cases} \dot{T}_s(x_{101}, t) = a_{3c}(t)T_s(x_{100}, t) + a_{2c}(t)T_s(x_{101}, t) + a_1(t)T_s(x_{102}, t) + \dfrac{P_\theta \psi(x_{101})}{\tau}\Delta Tad(t) \\ \dot{\widehat{\Delta T_{ad}}}(t) = \zeta(t) \\ \dot{\zeta}(t) = v(t) \end{cases} \tag{A2}$$

$$\begin{cases} \dot{T}_s(x_i, t) = a_3(t)T_s(x_{i-1}, t) + a_2(t)T_s(x_i, t) + a_1(t)T_s(x_{i+1}, t) + \dfrac{P_\theta \psi(x_i)}{\tau}\Delta Tad(t) \text{ for } 102 \le i \le 199 \\ \hat{T}_s(x_{200}, t)(t) = a_3(t)T_s(x_{199}, t) + a_5(t)T_s(x_{200}, t) + b_2(t)T_0 + b_3(t)q_{ext}(t) + \dfrac{P_\theta \psi(x_{200})}{\tau}\Delta Tad(t) \end{cases} \tag{A3}$$

This model can be written in the canonical form Eq. 14

$$
\begin{cases}
\dot{X}_1^1(t) = a_1(t)X_2^1(t) + G_1^1(X_1^1(t),\, T_0,\, t) \\
\dot{X}_2^1(t)(t) = a_1(t)X_3^1(t) + G_2^1(X_1^1(t),\, X_2^1(t),\, t) \\
\vdots \\
\dot{X}_{99}^1(t)(t) = a_1(t)X_{100}^1(t) + G_{99}^1(X_{99}^1(t),\, X_{98}^1(t),\, t) \\
\dot{X}_{100}^1(t)(t) = G_{100}^1(X_{99}^1(t),\, X_{100}^1(t),\, y_2(t),\, t) \\
\dot{X}_1^2(t) = r(t)X_2^2(t) + G_1^2(X_1^2(t),\, X_{99}^3(t),\, X_{100}^1(t),\, t) \\
\dot{X}_2^2(t) = X_3^2(t) \\
\dot{X}_3^2(t) = v(t) \\
\dot{X}_1^3(t) = a_3(t)X_2^3(t) + G_1^3(X_1^3(t),\, X_2^2(t),\, T_0,\, q_{ext},\, t) \\
\dot{X}_2^3(t)(t) = a_3(t)X_3^3(t) + G_2^3(X_1^3(t),\, X_2^3(t),\, X_2^2(t),\, t) \\
\vdots \\
\dot{X}_{98}^1(t)(t) = a_3(t)X_{99}^3(t) + G_{98}^3(X_{97}^3(t),\, X_{98}^3(t),\, X_2^2(t),\, t) \\
X_{99}^1(t)(t) = G_{99}^3(X_{98}^3(t),\, X_{99}^3(t),\, y_2(t),\, X_2^2(t),\, t) \\
y_1(t) = X_1^1(t) = T_s(x_1,\, t) \\
y_2(t) = X_1^2(t) = T_s(x_{101},\, t) \\
y_3(t) = X_1^3(t) = T_s(x_{200},\, t)
\end{cases}
\tag{A5}
$$

where

$$
r(t) = \frac{P_\theta \psi(x_{101})}{\tau}
$$

The G_i^j's vectors are given by

$$
G^1(X^1(t),\, T_0,\, y_2(t),\, t) = \begin{pmatrix} G_1^1(t) \\ G_2^1(t) \\ \vdots \\ G_{100}^1(t) \end{pmatrix}
= \begin{pmatrix} a_4(t)X_1^1(t) + b_1 T_0 \\ a_3(t)X_1^1(t) + a_2(t)X_2^1(t) \\ \vdots \\ a_3(t)X_{99}^1(t) + a_2(t)X_{100}^1(t) + a_1(t)y_2(t) \end{pmatrix} \tag{A6}
$$

where $y_2(t) = X_1^2(t) = T_s(x_{101},\, t)$

$$
G^2(X^2(t),\, X_{99}^3(t),\, X_{100}^1(t),\, t) = \begin{pmatrix} G_1^2(t) \\ G_2^2(t) \\ G_3^2(t) \end{pmatrix} \tag{A7}
$$

$$
G^2(X^2(t),\, X_{99}^3(t),\, X_{100}^1(t),\, t) = \begin{pmatrix} a_{3c}(t)X_{100}^1(t) + a_{2c}(t)X_1^2(t) + a_1(t)X_{99}^3(t) \\ 0 \\ 0 \end{pmatrix}
$$

$$
G^3(X^3(t),\, y_2(t),\, X_2^2(t),\, T_0,\, q_{ext},\, t) = \begin{pmatrix} G_1^3(t) \\ G_2^3(t) \\ \vdots \\ G_{99}^3(t) \end{pmatrix}
$$

$$
= \begin{pmatrix} a_5(t)X_1^3(t) + b_2(t)T_0 + b_3(t)q_{ext} \\ a_1(t)X_1^3(t) + a_2(t)X_2^3(t) \\ \vdots \\ a_1(t)X_{98}^3(t) + a_2(t)X_{99}^3(t) + a_3(t)y_2(t) \end{pmatrix}
+ \begin{pmatrix} \dfrac{P_\theta \psi(x_{200})}{\tau} X_2^2 \\ \dfrac{P_\theta \psi(x_{199})}{\tau} X_2^2 \\ \vdots \\ \dfrac{P_\theta \psi(x_{102})}{\tau} X_2^2 \end{pmatrix} \tag{A8}
$$

The coefficients a_i and b_i are given by

$$
a_1(t) = \frac{\lambda_{eff1}(t)}{(\Delta x_k)^2}, \quad a_2(t) = -2\frac{\lambda_{eff1}(t)}{(\Delta x_k)^2} + \frac{D(t)}{\Delta x_k},
$$

$$
a_3(t) = \frac{\lambda_{eff1}(t)}{(\Delta x_k)^2} - \frac{D(t)}{\Delta x_k},
$$

$$
a_4(t) = a_2(t) + a_3(t)\frac{\alpha(t)}{P_\theta \Delta x_1}\frac{1}{1 + \dfrac{\alpha(t)}{P_\theta \Delta x_1}},
$$

$$
a_5(t) = a_2(t) + a_1(t) \times \frac{1 + N' + \alpha^2(t)}{P_\theta \Delta x_2}\frac{1}{(1 + N')\left(1 + \dfrac{1}{P_\theta \Delta x_2}\right) + \dfrac{\alpha^2(t)}{P_\theta \Delta x_2} - \alpha(t)}.
$$

and

$$
a_{2c}(t) = (\Delta x_1 + \Delta x_2)\frac{\lambda_{eff1}(t)}{\Delta x_1 (\Delta x_2)^2} + \frac{D(t)}{\Delta x_1},
$$

$$
a_{3c}(t) = \frac{\lambda_{eff1}(t)}{(\Delta x_1)(\Delta x_2)} - \frac{D(t)}{\Delta x_1},
$$

$$
b_1(t) = a_3(t)\frac{1}{1 + \dfrac{\alpha(t)}{P_\theta \Delta x_1}},
$$

$$
b_2(t) = a_1(t)\frac{1 + N' - \alpha(t)}{(1 + N')\left(1 + \dfrac{1}{P_\theta \Delta x_2}\right) + \dfrac{\alpha^2(t)}{P_\theta \Delta x_2} - \alpha(t)}
$$

and

$$
b_3(t) = a_1(t)\frac{1}{\rho_0 u_{v0} c_{pmg} S}\frac{1}{(1 + N')\left(1 + \dfrac{1}{P_\theta \Delta x_2}\right) + \dfrac{\alpha^2(t)}{P_\theta \Delta x_2} - \alpha(t)}
$$

with

$$D(t) = \frac{1 - \alpha(t)}{2\tau},\ \lambda_{eff1}(t) = \frac{1}{\tau P_{\alpha x\theta}} + \frac{1 + \alpha^2(t)}{2P_\theta \tau}$$

and

$$\Delta x_k = \Delta x_1 = 8.3651.10^{-3}, \quad \Delta x_k = \Delta x_2 = 1.5513.10^{-3}$$

are respective subinterval in the inert monolith and the catalytic monolith.

Proof of the convergence of the observer (Eq. 15)

First, let us recall some existing results [see Gauthier et al., 1992; Deza et al., 1992; Farza et al., 1998; Hammouri et al., 2002). Consider the single output system

$$\begin{cases} \dot{x}(t) = A(t)x(t) + \varphi(t, x) \\ y(t) = Cx(t) = x_1(t) \end{cases} \tag{A9}$$

Here the state of the system is

$$x(t) = \begin{pmatrix} x_1(t) \\ \vdots \\ x_n(t) \end{pmatrix}$$

and

$$A(t) = a(t)\begin{pmatrix} 0 & 1 & 0 & 0 \\ \vdots & \ddots & \ddots & 0 \\ 0 & \cdots & \ddots & 1 \\ 0 & \cdots & \cdots & 0 \end{pmatrix};\ C_1 = (1 \quad 0 \ldots 0)$$

The i^{th} component φ_i of φ satisfies the following triangular expression $\varphi_i(t, x) = \varphi_i(t, x_1(t), \ldots, x_i(t))$, it means that φ_i depends at most on $(x_1, \ldots, x_i)$. Assuming that φ_i is global Lipschitz w.r.t x it means that there exists a constant $c > 0$, such that, $\|\varphi_i(t, x) - \varphi_i(t, x')\| \leq c\|x - x'\|$, where $\|x - x'\| = \sqrt{(x_1 - x'_1)^2 + \cdots + (x_n - x'_n)^2}$. These global Lipschitz assumptions can be omitted in the case where the state $x(t)$ of the system is bounded. Consider,

$$K = \begin{pmatrix} k_1 \\ \vdots \\ k_n \end{pmatrix}$$

such that all eigenvalues of the $n \times n$ matrix

$$\begin{pmatrix} k_1 & 1 & 0 & \cdots & 0 \\ \vdots & \ddots & \ddots & \ddots & \vdots \\ k_{n-1} & 0 & \cdots & 0 & 1 \\ k_n & 0 & \cdots & 0 & 0 \end{pmatrix}$$

lie into the left half plane

$\mathbb{C}^- = \{\lambda \in \mathbb{C}/\mathrm{Re}(\lambda) < 0\}$ (where $\mathrm{Re}(\lambda)$ denotes the real part of the complex number λ).

Now set

$$\Theta = \begin{pmatrix} \Omega & 0 & \cdots & 0 \\ 0 & \Omega^2 & \ddots & \vdots \\ \vdots & \ddots & \ddots & 0 \\ 0 & \cdots & 0 & \Omega^n \end{pmatrix},$$

where $\Omega \geq 1$ is a fixed parameter. Under the above notations, an observer for system 23 takes the form

$$\dot{\hat{x}}(t) = A(t)\hat{x}(t) + \varphi(t, \hat{x}(t)) + a(t)\Theta K(\widehat{x_1}(t) - y(t)) \tag{A10}$$

This observer converges exponentially for Ω sufficiently large: this means that $\|\hat{x}(t) - x(t)\| \leq \mu e^{-\nu t}\|\hat{x}(0) - x(0)\|$, where $\mu > 0$ and $\nu > 0$ are constants.

It is now shown that system 15 is an observer for system 14. Consider the following subsystem of Eq. 14

$$\begin{cases} \dot{X}^1(t) = A^1(t)X^1(t) + G^1(X^1(t), y_2(t), T_0, t) \\ y_1(t) = C_1X^1(t) = X_1^1(t) \end{cases} \tag{A11}$$

where $A^1(t)$, G^1 and C_1 are those defined in system 14. Note that the system has a similar triangular structure as system A9. Consequently, an observer for Eq. A11 takes the form

$$\dot{\hat{X}}^1(t) = A^1(t)\hat{X}^1(t) + G^1(\hat{X}^1(t), y_2(t), T_0, t) + a_1(t)\Theta_1K^1(\hat{X}_1^1(t) - y_1(t)) \tag{A12}$$

where

$$K^1 = \begin{pmatrix} K_1^1 \\ \vdots \\ K_{100}^1 \end{pmatrix}$$

is such that the matrices

$$\bar{A}^1 = \begin{pmatrix} K_1^1 & 1 & 0 & 0 \\ \vdots & 0 & \ddots & \vdots \\ K_{99}^1 & 0 & \cdots & 1 \\ K_{100}^1 & 0 & \cdots & 0 \end{pmatrix}$$

is stable (it means that eigenvalues of the $\bar{A}^i$'s belong to the left half plane ($\mathbb{C}^-$)) and Θ_1 is given by

$$\Theta_1 = \begin{pmatrix} \Omega & 0 & 0 \\ 0 & \ddots & 0 \\ 0 & 0 & \Omega^{100} \end{pmatrix}$$

Thus, $\hat{X}^1(t)$ converges exponentially to $X^1(t)$. This estimator gives the temperature profile in the inert monolith.

Now, consider the problem of estimation of ΔT_{ad}. The corresponding model is

$$\begin{cases} \dot{X}^2(t) = A^2(t)X^2(t) + G^2(X^2(t), X_{99}^3(t), X_{100}^1(t), t) + v(t)B \\ y_2(t) = C_2X^2(t) = X_1^2(t) \end{cases} \tag{A13}$$

with

$$B = \begin{pmatrix} 0 \\ 0 \\ 1 \end{pmatrix}; \; C_2 = (1 \quad 0 \quad 0)$$

where $v(t)$ is an unknown input. Recall that

$$A^2(t) = \begin{pmatrix} 0 & r(t) & 0 \\ 0 & 0 & 1 \\ 0 & 0 & 0 \end{pmatrix}$$

Now, consider the following change of variables $\widetilde{X_1^2}(t) = X_1^2(t)$, $\widetilde{X_2^2}(t) = r(t)X_2^2(t)$, and $\widetilde{X_3^2}(t) = r(t)X_3^2(t)$. This means that $X^2(t) = \Lambda(t)\tilde{X}^2(t)$ or equivalently $\tilde{X}^2(t) = \Lambda^{-1}(t)X^2(t)$, where

$$\Lambda^{-1}(t) = \begin{pmatrix} 1 & 0 & 0 \\ 0 & r(t) & 0 \\ 0 & 0 & r(t) \end{pmatrix}$$

From these notations, we get

$$\dot{\tilde{X}}^2(t) = \tilde{A}^2(t)\widetilde{X^2}(t) + \widetilde{G^2}(\widetilde{X^2}(t), X_{99}^3(t), X_{100}^1(t), t) + r(t)v(t)B \tag{A14}$$

where

$$\tilde{A}^2(t) = \begin{pmatrix} 0 & 1 & 0 \\ 0 & 0 & 1 \\ 0 & 0 & 0 \end{pmatrix}$$

and

$$\widetilde{G^2}(\widetilde{X^2}(t), X_{99}^3(t), X_{100}^1(t), t) = G^2(\Lambda^{-1}(t)X^2, X_{99}^3(t), X_{100}^1(t), t) + 1/r(t)\begin{pmatrix} 0 \\ \dot{r}\widetilde{X_2^2}(t) \\ \dot{r}\widetilde{X_3^2}(t) \end{pmatrix}$$

Since G^2 has a triangular structure with respect to $X^2(t)$, it follows that $\widetilde{G^2}(t)$ has also a triangular structure w.r.t. $\widetilde{X^2}(t)$, and then if $X_{99}^3(t)$ is assumed to be known, and because, $\hat{X}_{100}^1(t)$ converges exponentially to $X_{100}^1(t)$, from above (Eq. A10), an observer for $\widetilde{X^2}(t)$ takes the form

$$\dot{\hat{\tilde{X}}}^2(t) = \tilde{A}(t)\hat{\tilde{X}}^2(t) + \widetilde{G^2}(\hat{\tilde{X}}^2(t), X_{99}^3(t), \hat{X}_{100}^1(t), t) + \Theta_2 K^2(\hat{\tilde{X}}_1^2(t) - y_2(t)) \tag{A15}$$

where

$$K^2 = \begin{pmatrix} K_1^2 \\ K_2^2 \\ K_3^2 \end{pmatrix}$$

is such that all the eigenvalues of

$$\begin{pmatrix} K_1^2 & 1 & 0 \\ K_2^2 & 0 & 1 \\ K_3^2 & 0 & 0 \end{pmatrix}$$

are in $\mathbb{C}^-$ and

$$\Theta_2 = \begin{pmatrix} \Omega & 0 & 0 \\ 0 & \Omega^2 & 0 \\ 0 & 0 & \Omega^3 \end{pmatrix}$$

Thus, an observer permitting to estimate $X^2(t)$ is given by

$$\dot{\hat{X}}^2(t) = A^2(t)\hat{X}^2(t) + G^2(\hat{X}^2(t), X_{99}^3(t), \hat{X}_{100}^1(t), t) + \Lambda(t)\Theta_2 K^2(\hat{\tilde{X}}_1^2(t) - y_2(t)) \tag{A16}$$

More precisely, $\|\hat{X}^2(t) - X^2(t)\| \leq \alpha e^{-\beta t}\|\hat{X}^2(0) - X^2(0)\| + \delta$ where $\alpha > 0$ and $\beta > 0$ are constants, and δ is a constant depending on the upper bound of $|v(t)|$ and on the parameter of calibration Ω. Moreover, δ can be rendered small by taking Ω large (see Hammouri et al., 2002 for more details).

This observer is based on the fact that X_{99}^3 is known. In practice, this variable is not a measured one, this is why X_{99}^3 must be replaced in (Eq. A16) by $\hat{X}_{99}^3$, coming from the following estimator

$$\dot{\hat{X}}^3(t) = A^3(t)\hat{X}^3(t) + G^3(\hat{X}^3(t), \hat{X}_2^2(t), T_0, q_{ext}, y_2(t), t) + a_3(t)\Theta_3 K^3(\hat{X}_1^3(t) - y_3(t)) \tag{A17}$$

This last observer is constructed in a similar way as above, where

$$K^3 = \begin{pmatrix} K_1^3 \\ \vdots \\ K_{99}^3 \end{pmatrix}$$

is such that the eigenvalues of

$$\begin{pmatrix} K_1^3 & 1 & 0 & 0 \\ \vdots & 0 & \ddots & \vdots \\ K_{98}^3 & 0 & \cdots & 1 \\ K_{99}^3 & 0 & \cdots & 0 \end{pmatrix}$$

lie in $\mathbb{C}^-$, and Θ_3 is given by

$$\begin{pmatrix} \Omega & 0 & 0 \\ 0 & \ddots & 0 \\ 0 & 0 & \Omega^{99} \end{pmatrix}.$$

Manuscript received May 7, 2003, and revision received Sept. 10, 2003.